GEOPHYSICS, VOL. XXIX, NO. 5 (OCTOBER, 1964), PP. 783-805, 15 FIGS.

A NEW DATA-PROCESSING TECHNIQUE FOR THE ELIMINATION OF GHOST ARRIVALS ON REFLECTION SEISMOGRAMS†

WILLIAM A. SCHNEIDER,* KENNETH L. LARNER,‡ J. P. BURG,* AND MILO M. BACKUS*

A new data-processing technique is presented for the separation of initially up-traveling (ghost) energy from initially down-traveling (primary) energy on reflection seismograms. The method combines records from two or more shot depths after prefiltering each record with a different filter. The filters are designed on a least-mean-square-error criterion to extract primary reflections in the presence of ghost reflections and random noise. Filter design is dependent only on the difference in uphole time between shots, and is independent of the details of near-surface layering. The method achieves wide-band separation of primary and ghost energy, which results in 10–15 db greater attenuation of ghost reflections than can be achieved with conventional two- or three-shot stacking (no prefiltering) for ghost elimination.

The technique is illustrated in terms of both synthetic and field examples. The deghosted field data are used to study the near-surface reflection response by computing the optimum linear filter to transform the deghosted trace back into the original ghosted trace. The impulse response of this filter embodies the effects of the near-surface on the reflection seismogram, i.e. the cause of the ghosting. Analysis of these filters reveals that the ghosting mechanism in the field test area consists of both a surface- and base-of-weathering layer reflector.

INTRODUCTION

In exploration seismology when an explosive source is detonated below the free surface, the initial up-traveling energy is either absorbed or returned to the subsurface by the near-surface reflection complex. If the reflected energy forms a coherent wavefront, then we may expect to record both primary and ghost arrivals from every reflector at depth, separated in time by approximately twice the traveltime from the shot to the near-surface reflection complex. This "double image" view of the subsurface which results from ghosting is clearly undesirable for the following reasons:

(1) Doubling the number of reflection events on the record compounds the subsurface interpretation.

(2) Ghosts and primaries may interfere destructively, thereby masking subsurface information.

(3) The ghost-reflection interference may vary considerably within a prospect, causing poor character correlation.

The latter is perhaps the most undesirable feature of ghosting. Since the ghost reflections are sensitive to near-surface conditions in the vicinity of the shotpoint, such as thickness of the weathering layer, roughness of surface and base-of-weathering reflector, depth of the shot, position of water table, to mention a few, we might well expect ghosting to vary significantly within short lateral distances. This variation in the ghosting can destroy meaningful fine structure in the primary reflections which may convey stratigraphic trap information. For these as well as other reasons, ghost arrivals are classified as seismic noise along with surface waves, multiple reflections, scattered energy, wind noise, etc.

The elimination of ghost energy from seismic records may be accomplished by exploiting the space-time relationship between primary and ghost arrivals on a single or multichannel basis. An example of the former is provided in Lindsey's (1960) article whereby a simple positive feedback loop is employed to effectively cancel ghosts from a single near-surface reflector against

† Presented at the 32nd Annual International SEG Meeting, Calgary, Alberta, Canada, September 19, 1962; Pacific Section AAPG, SEG, and SEPM, Los Angeles, April 25, 1963. Manuscript received by the Editor July 3, 1963.

* Texas Instruments Incorporated, Dallas, Texas.

‡ Graduate Student, Massachusetts Institute of Technology, Department of Geology and Geophysics, Cambridge, Massachusetts.

primaries. In Lindsey's notation, the filter to apply to each trace is given by

$$\frac{1}{(1 - aH(s)e^{-s\tau})} \qquad (1)$$

a = near-surface reflection coefficient.
$H(s)$ = near-surface filter to account for differences in primary and ghost wavelet.
τ = delay between primary and ghost.
s = Laplace-transform variable.

As is evident from equation (1) this method of ghost rejection requires specific and detailed information about the ghosting mechanism, which, in all but the simplest cases, is difficult to obtain from the field records. As Lindsey demonstrates, the autocorrelation function of the input data may in principle furnish the parameters a, $H(s)$, and (τ) with sufficient accuracy for the feedback technique to be employed. This requires, however, (1) a high signal-to-noise ratio, (2) wide-band signal information, and (3) a simple total seismic system wavelet. Any significant amplitude in the correlation function due to the primaries themselves at other than zero lag would seriously hamper isolating that part of the correlation due to ghosting, and the specification of the parameters for equation (1). This will become evident in the following.

The multichannel techniques currently available for ghost elimination consist of vertical shot stacking (Hammond, 1962), and the use of distributed charges (Musgrave, Ehlert, and Nash, 1958; Sparks and Silverman, 1953). These, of course, differ only in degree and not kind as they both represent vertical stacking. The philosophy of vertical shot stacking, for ghost elimination, finds its basis in the time relationship that exists between primaries and ghosts from different shot depths. If we have several shots at different depths recorded at the same seismometer position, and static correct these traces to a common shot depth, the primary reflections will time tie and the ghosts, of course, will not. By stacking the time-shifted traces, it is clear that the primary energy will be enhanced relative to the ghost energy. The stacking may be accomplished in the playback center with the individually recorded shots, or in the field with delayed charges or distributed charges whose detonation velocity is matched to the propagation velocity of the surrounding medium. This is a brute-force ghost-cancellation technique which works the ghost reflections against themselves. It is attractive in that it does not require knowledge of the ghosting mechanism or the primary-ghost relationship. The major shortcoming of the conventional shot-stacking scheme results from its narrow-band rejection capability when stacking only a few shots. This limitation is serious for two reasons: (1) There is an industry-wide movement to achieve wide-band seismic reflection data for fuller utilization of the available signal spectrum; therefore, narrow-band techniques are decidedly undesirable if alternatives exist; (2) The narrow-band rejection capability makes the shot separation a critical parameter; the shot spacing must be very nearly $\frac{1}{4}$ wavelength for the peak frequency in the spectrum of the ghost wavelet in order to deghost successfully even with narrow-band input.

These considerations lead us to the conclusion that the ideal ghost-elimination processor should require: (1) both wide-band ghost rejection and signal preservation capabilities, and (2) minimum knowledge of the ghosting mechanism and the primary-ghost relationship. These requirements can be well met by allowing for individually filtering the several shots before stacking as is demonstrated in the following.

METHOD

This multichannel-processing technique is schematically characterized below.

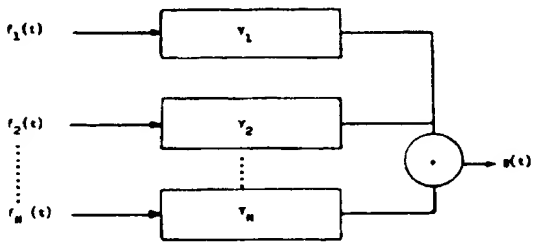

Where $f_i(t)$ is the input trace from the ith shot at a given seismometer location, the Y_i's are filters applied to the traces before summation, and $g(t)$ is the output of the processor.

The complex transfer functions $Y_i(f)$ are designed, on a least-mean-square-error criterion, to extract primary events from random noise and ghost events, on the basis of the differential time dependence of primaries and ghosts on hole

depth. The least-squares-filter design is p d in Appendix A.

Although any number of shots can be stacked by this process, two shots usually provide ample attenuation of the ghost energy. Therefore, we will restrict our attenuation to two-channel processes.

In the specification of the signal and noise model it is assumed that the signal and noise are statistically independent. This assumption insures that the resulting filters $Y_1(f)$ and $Y_2(f)$ will not require knowledge of the ghosting mechanism for their specification. The fact that the primaries and ghosts are in fact correlated does not invalidate the process, but rather reflects that we are not using all the information in the data available to us. By utilizing this latter correlation we could obtain a somewhat more effective deghosting processor. However, the difficulty in estimating the primary-ghost correlation and the impracticality of having to redesign the filters for each new ghosting situation presently outweighs any potential gain. Before proceeding to examine specific examples of the use of the processor, it is instructive to compare its theoretical response with that of the conventional shot-stacking technique. The parameter of interest here is the ratio of (ghost/primary) amplitude response as a function of frequency. Clearly, we desire this to be as small as possible consistent with signal preservation and random noise rejection at all frequencies. If we define the signal and noise for the two shots as

$$S_1(t) = P(t)$$

(primary arrivals from shallow shot)

$$S_2(t) = P(t)$$

(primary arrivals from deep shot)

and

$$N_1(t) = G(t)$$

(ghost arrivals from shallow shot)

$$N_2(t) = G(t - \Delta t)$$

(ghost arrival from deep shot)

where Δt is the ghost reflection moveout between the two shots after static correcting the traces to a common depth, and equals twice the difference in uphole ($2\Delta t_{uh}$) time; then the responses for primaries and ghosts for the conventional are, respectively,

$$S_1(t) + S_2(t) = 2P(t)$$
$$N_1(t) + N_2(t) = G(t) + G(t - \Delta t). \quad (2)$$

Transforming equation (2) to the frequency domain we have

response for primaries

$$= 2\bar{P}(f)$$

response for ghosts

$$= \bar{G}(f)(1 + e^{-i2\pi f\Delta t}), \quad (3)$$

where

$$\bar{x}(f) = \int_{-\infty}^{\infty} x(t)e^{-i2\pi ft}dt$$

and

$$x(t) = \int_{-\infty}^{\infty} \bar{x}(f)e^{i2\pi ft}df$$

are Fourier-transform pairs.

From equation (3), the transfer function of the conventional stack process for primary events is the constant 2, and for ghosts $(1+e^{-i2\pi f\Delta t})$. The amplitude of the ratio of ghost-to-primary-transfer functions is clearly

$$|\cos \pi f\Delta t|, \quad (4)$$

a well-known result.

Similarly, the responses for primaries and ghosts for the present process, which we call "Optimum Wide-Band Stack" process, are, respectively,

response for primaries

$$= \bar{P}(f)(Y_1(f) + Y_2(f))$$

response for ghosts

$$= \bar{G}(f)(Y_1(f) + Y_2(f)e^{-i2\pi f\Delta t})$$

and the amplitude of the ratio of ghost-to-primary-transfer functions is

$$\frac{|Y_1(f) + Y_2(f)|}{|Y_1(f) + Y_2(f)e^{-i2\pi f\Delta t}|}. \quad (5)$$

Expressions (4) and (5) are plotted in Figure 1. The difference in the breadth of the reject bands

of the two processes is apparent. In particular, for a ΔT of 10 msec, the -20 db reject range for the conventional two-shot stack is only 47 to 53 cps, whereas the present process provides a 20–80 cps range. The latter increased the rejection bandwidth by a factor of 10 over the conventional two-channel stack. This difference, as well as the general effectiveness of the method, is best illustrated in the following deghosting examples using both synthetic and field examples.

RESULTS

The first example is a highly idealized synthetic case, but it serves to put the results of Figure 1 in the more familiar light of wavelets that might be expected to occur on a reflection seismogram.

Figure 2 shows the idealized cross section including shot and recording geometry used to combat ghost reflections on a multichannel basis. Two or more shots are recorded at each seismometer group for stacking purposes. The shot separation is determined by a rough knowledge of the velocity in the shot interval, and the center frequency of the signal spectrum.

Figure 3 depicts a possible pr , and ghost reflection resulting from the shots A and B recorded at one seismometer group. The traces A and B have been time-shifted to a common shot depth, thereby lining up primary events. The ghost reflections in this case show a 10-msec moveout or a difference in uphole time $\Delta T_{uA} = 5$ msec. The figure also shows a comparison of the conventional stack and the present system for ghost rejection. The former method simply adds the two traces with a resulting attenuation of ghost amplitude of about -7 db, while the latter filters each trace with different filters and then stacks, achieving in this instance better than -25 db rejection of the ghost energy.

The primary and ghost wavelets in this example are identical but reversed in polarity. Their amplitude spectrum is given by

$$\overline{P(f)} = \left(1 - \cos\frac{2\pi f}{100}\right) \qquad 0 < f \leq 100$$

$$\overline{P(f)} = 0 \qquad f > 100 \text{ cps},$$

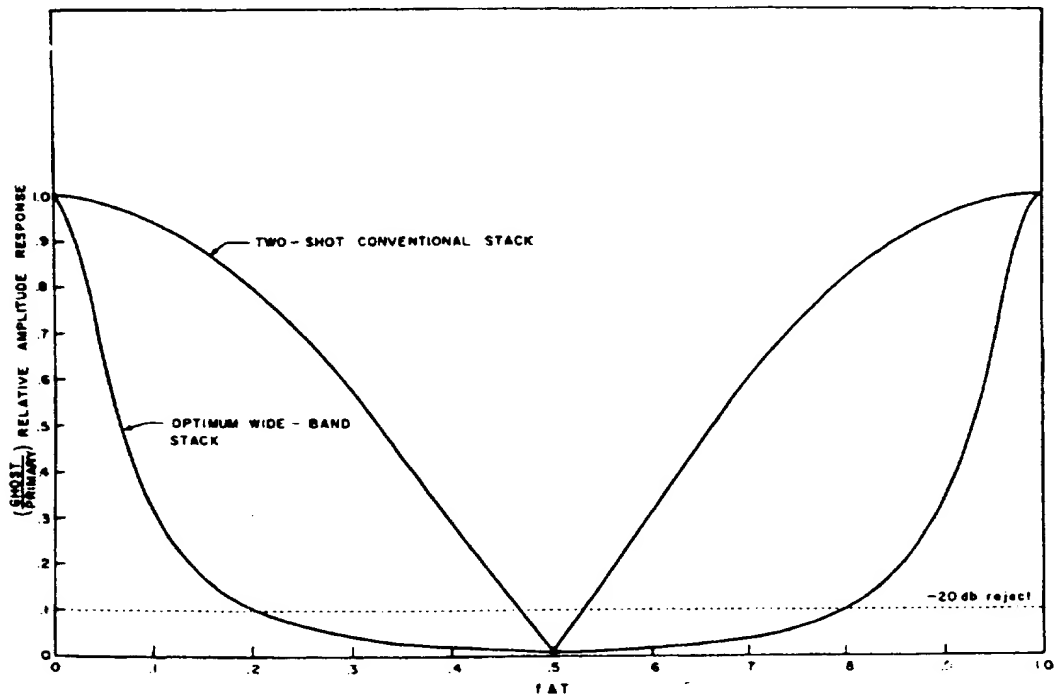

FIG. 1. Comparison of the present process and conventional two-shot stack response for primary and ghost energy.

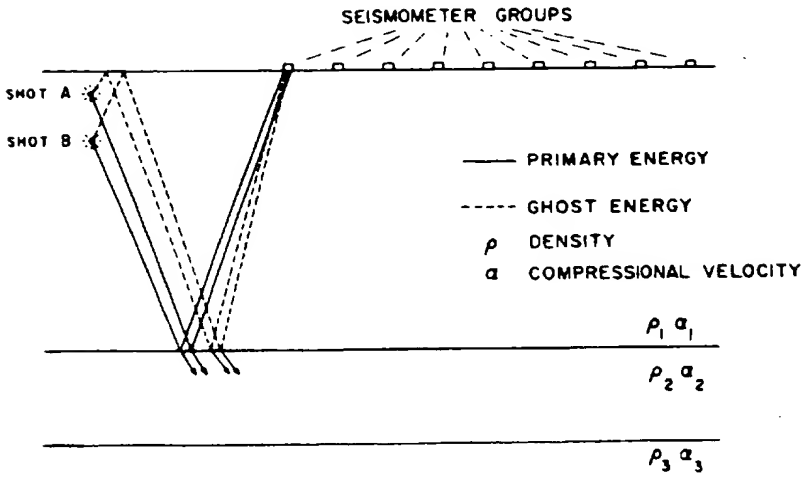

FIG. 2. Idealized ghost problem in reflection seismology.

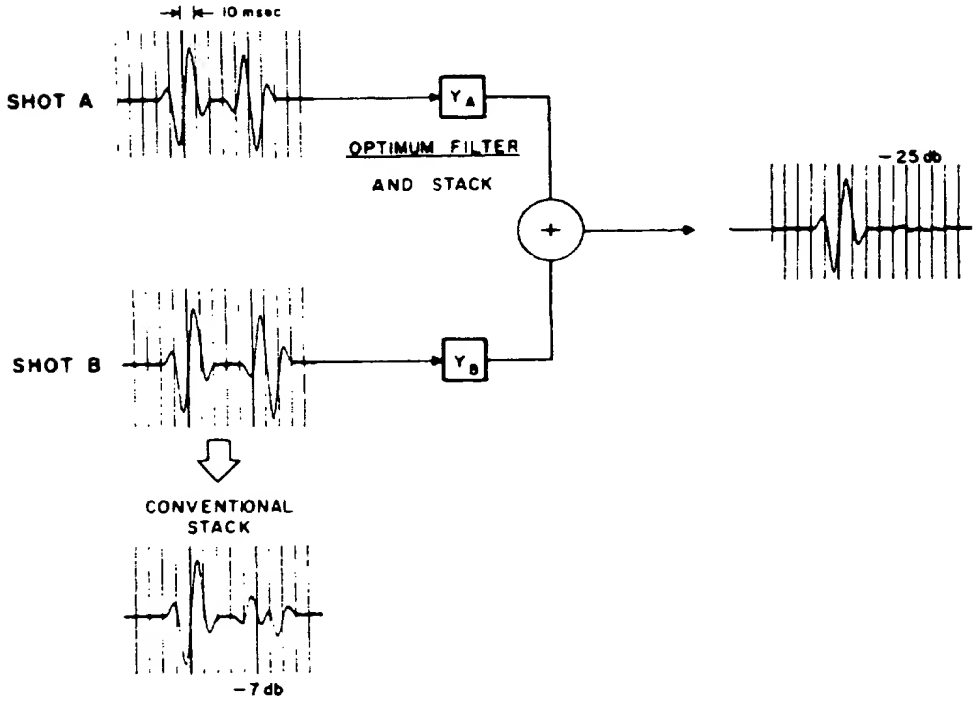

FIG. 3. Comparison of the present process and conventional stack for ghost elimination utilizing synthetic wavelets.

which is peaked at 50 cps. With ΔT = 10 msec for the ghost wavelets, it is evident that this spectrum would have its peak frequency centered at $f_{peak} \cdot \Delta T = .5$ in Figure 1. Thus, the results in Figure 3 represent the maximum rejection possible for either process using this wavelet. The advantages of the wide-band rejection and signal-preservation characteristics of the process are self-evident. In addition, no specific knowledge of the primary-ghost relationship or the spectrum of the wavelets, other than the $\Delta T = 2\Delta T_{uA}$, is required to implement the filters Y_A and Y_B. Fortunately, the difference in uphole time can be obtained accurately in the field with little difficulty if reasonable care is taken to record an uphole pulse with each shot. Other data which can provide an independent check on the ΔT are: (1) accurate knowledge of the shot separation and vertical velocity in that depth increment, (2) correlation functions, (3) difference of arrival times of both primaries and ghost from shots at different depths.

The second example uses field data taken from an uphole survey near Sherman, Texas.

The spread geometry and details of the uphole survey are shown in Figure 4. Two holes were shot from 180 ft to 40 ft in 20-ft increments using 5-lb charges. The recording array was designed to reject the prominent surface waves, based on previous noise studies in the area. Only 12 of the available 24 channels were used on the surface spread; the remaining 12 were employed with a vertical array of seismometers cemented in the ground as part of an auxiliary study. Programmed gain control and a recording passband of 10–350 cps were employed.

The upper half of Figure 5 shows the center four traces obtained from SP 2 at the 180-ft and 160-ft shot depths. They have been corrected for normal moveout and static corrected to the deeper shot. Several strong reflection complexes are evident from .2–.4 sec and commencing again at about 1.3 sec. The shallow marker at .31 sec, and the first part of the reflection complex at about 1.4 sec, correlate well between records from different shot depths indicating these events are primaries (solid circles); however, the remainder of the reflections do not have good character correlation nor do they necessarily time-tie. This is particularly evident for the events between .34–.40 sec. They lag the primary at .31 sec by less than or equal to $2T_{uA}$, or 82 and 76 msec for the 180-ft and 160-ft shots, respectively. As will be demonstrated, these events are ghost reflections from the base of the weathering (open circles) and surface reflectors.

The lower half of Figure 5 shows the results of conventional and optimum wide-band shot stacking of the 180-ft and 160-ft records. The results of the conventional stack indicate fair improvement in ghost reduction over the input traces directly above. This is predictable from the two-shot-stack response for ghost energy in Figure 1. The reflection peak frequency of the records varies from about 50 cps for the early events to about 30 cps for the later arrivals. The ghost moveout for the 20-ft shot interval is about 6 msec as can be seen from the records. Therefore, the product $F_{peak}\Delta T$ in Figure 1 ranges between .18 and .30 giving predicted ghost rejection of about 3–6 db. The actual achieved rejection appears to be slightly less than this. The optimum wide-band stack results shown in the last 12 traces indicate that ghost energy has been attenuated of the order of 10–20 db, which is in general agreement with the response curves of Figure 1 for the frequencies and moveout involved. In particular, it is noted that the low-frequency "leggy" portion of the deep reflector at 1.5 sec is, in fact, ghost energy. This is unattenuated by the conventional stack, but is well rejected by the present process. Both shot-stacking processes represented in Figure 5 preserve signal (primary) amplitude and waveform, but they differ markedly in their rejection capabilities. Furthermore, the only information necessary for the implementation of the present process was the ghost moveout, or twice the difference in uphole times = 6 msec.

The very nature of ghosting makes its *positive* identification on the basis of one shot depth almost impossible, even though the ghost reflections may be strong. It is felt this is the primary reason that the importance of ghost reflections has been a somewhat controversial subject in reflection seismology. If, however, the seismogram is viewed as a function of shot depth, the primary and ghost energy are clearly separable on the basis of their arrival-time relationship. To illustrate this, a representative trace from each shot depth at SP 2 was gathered onto one record to facilitate the shot depth comparison. Rather than select a particular trace from each depth, however, a velocity filter (Embree, Burg, and

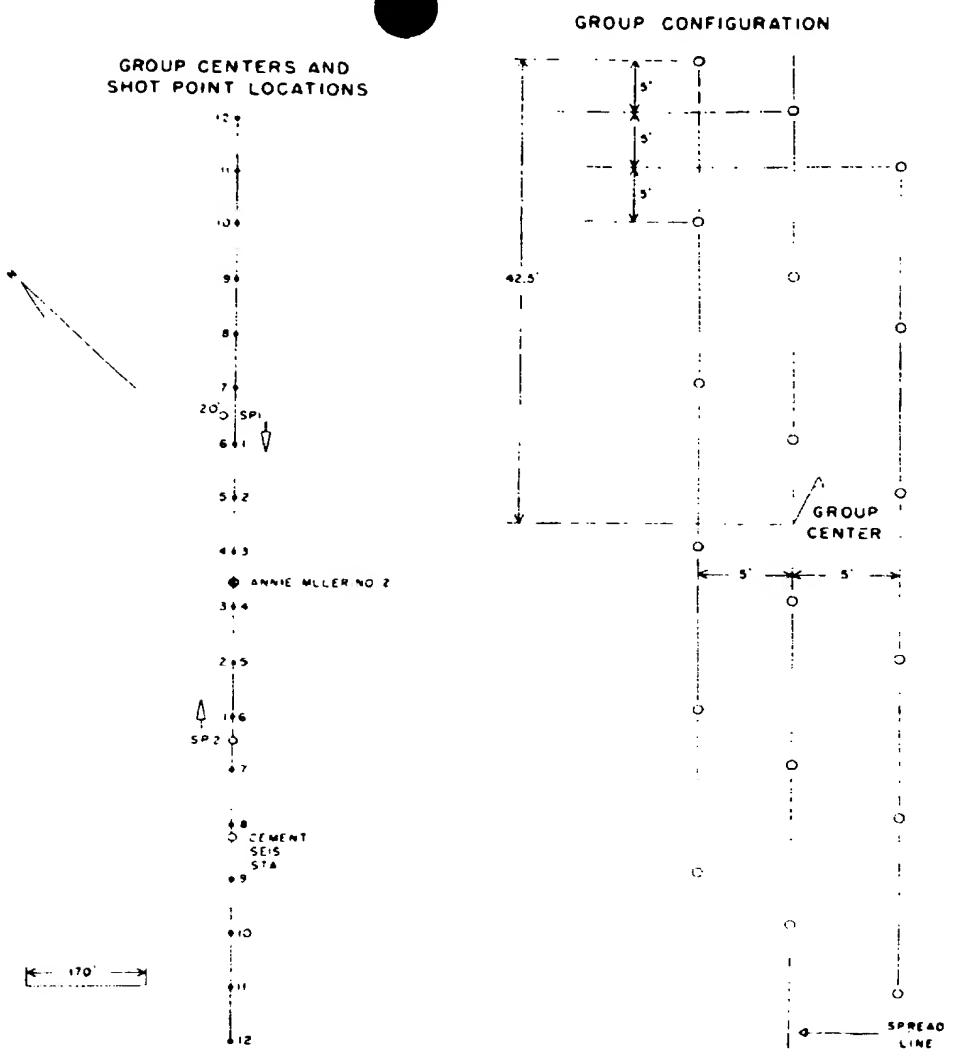

FIG. 4. Spread configuration for uphole survey taken near Sherman, Texas.

Backus, 1963) was applied to each 12-trace record to yield a single-trace representation of each shot depth. The application of the velocity filter here achieved additional rejection of the horizontally travelling shot-generated noise that was not cut out by the seismometer groups. Thus, each single trace representation is essentially free of horizontally traveling energy. What remains is composed of primaries, multiples, ghosts, and any scattered energy with less than two msec per trace moveout across the spread.

The gathered traces are shown in Figure 6 as the top eight traces. They have not been static corrected to a common depth. Therefore, primaries will arrive earlier from the deep than from the shallow shots while the opposite is true for ghosts. The presence of both primary and ghost moveout is evident with the formation of the characteristic "V" pattern due to generically related primaries and ghosts. Several of these can be seen at record times of .34 sec, 1.45 sec, 1.7 sec, and 1.86 sec. There can be no doubt on this

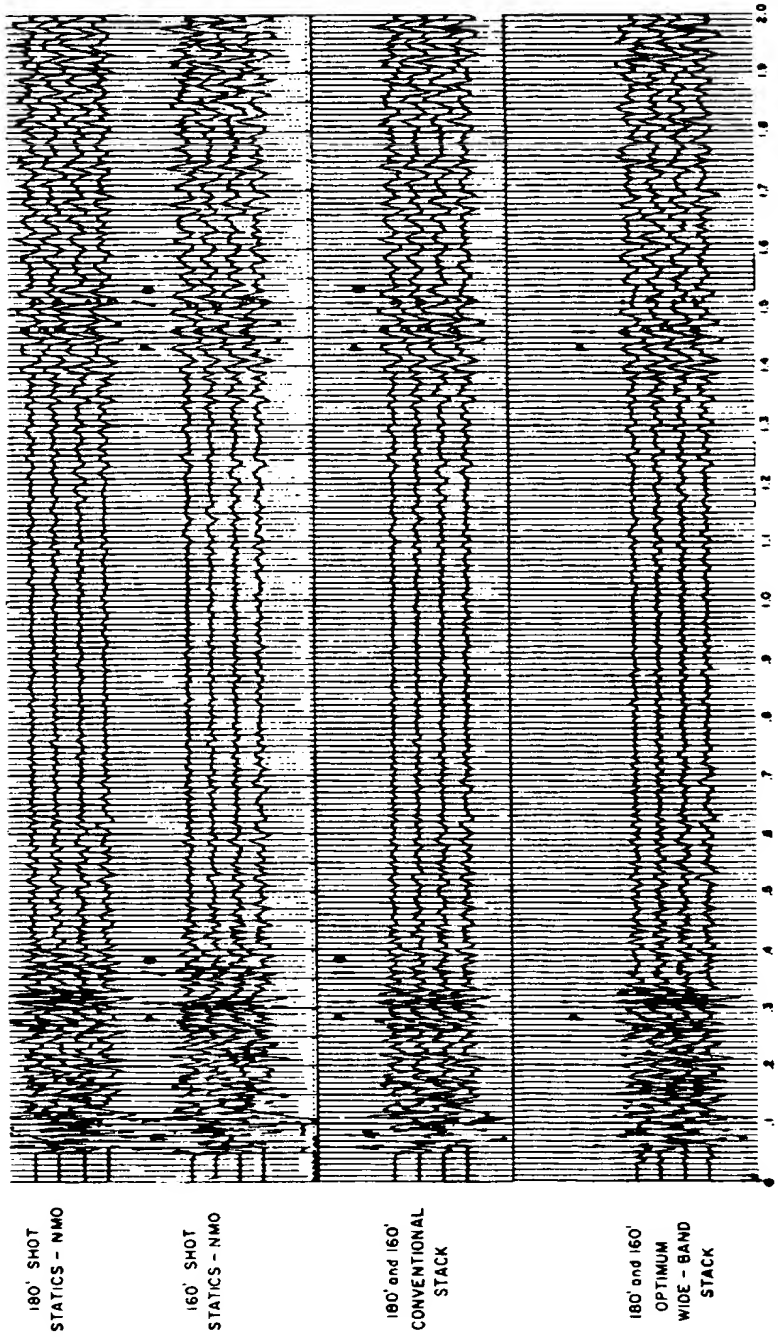

FIG. 5. 180-ft and 160-ft shot records before and after stacking.

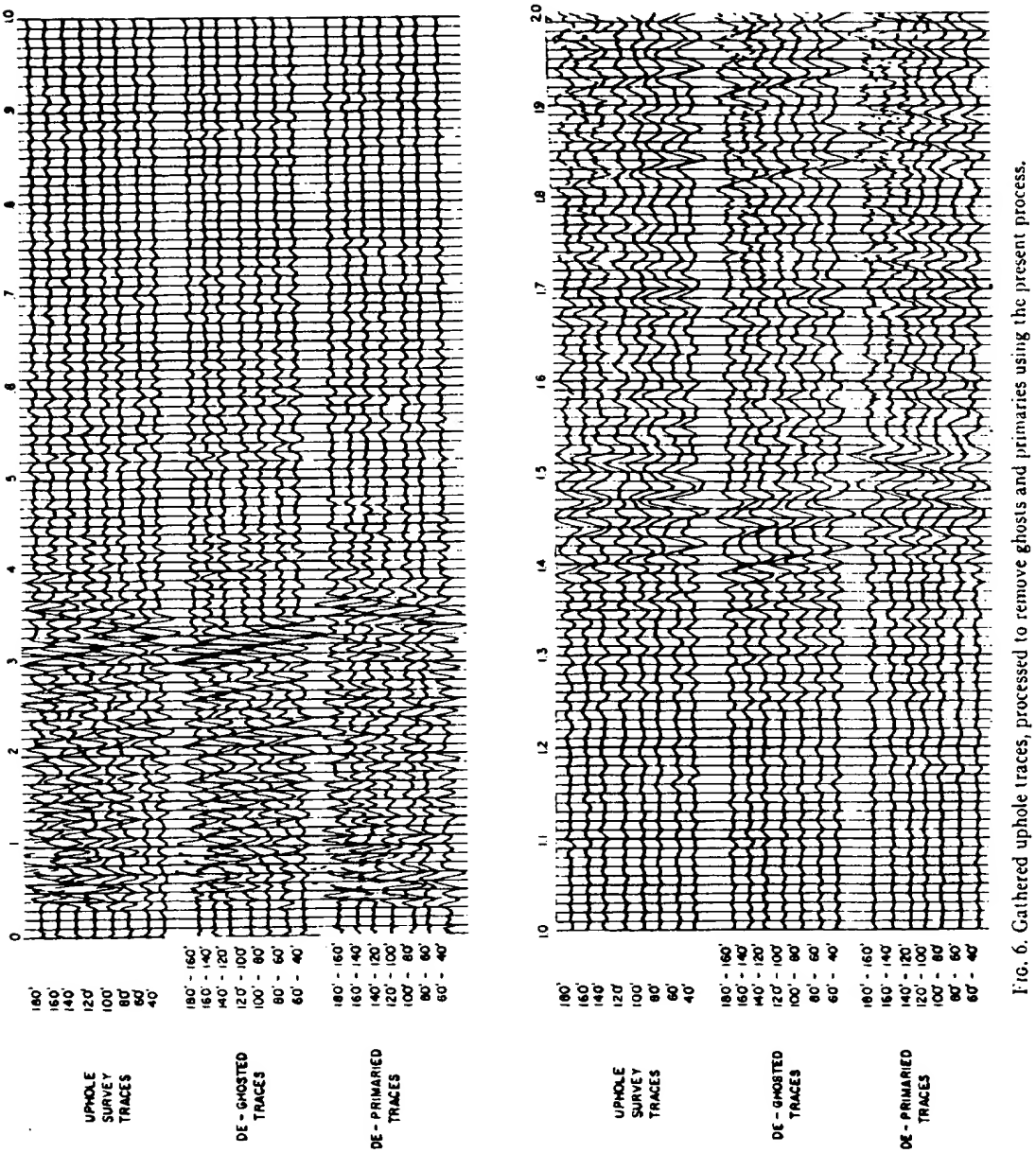

Fig. 6. Gathered uphole traces, processed to remove ghosts and primaries using the present process.

type of a display that ghost energy [redacted] both present and strong, whereas single depth information would not be nearly as revealing. The effect of shot depth on character correlation when ghost energy is present can best be seen in the reflection complex at about 1.45 sec. Notice the drastic changes in waveform across the 140 feet of shot depth resulting from primary-ghost interference. Similar horizontal variations also can be expected in the primary-ghost relationship for reasons previously mentioned. The removal of this ghost interference is mandatory before meaningful significance can be attached to reflection waveforms. The present process was applied to adjacent pairs of uphole traces resulting in the deghosted traces immediately below them in Figure 6. The first deghosted trace results from "optimum stacking" the 180-ft and 160-ft traces, etc. The most striking result is that the deghosted traces show only primary moveout. The obvious ghost-picks on the input traces have completely vanished for visual purposes, which implies about -20 db rejection. Other significant features are: (1) Several shallow reflections have been enhanced. (2) A number of weak reflectors in the quiet zone .35–1.2 sec have become pickable, (3) Character correlation is excellent across the 140 ft of shot depth. The latter is particularly noticeable at about 1.4 sec where the correlation is equally good for the high-frequency reflection sequence onset as it is for the low-frequency tail. This again illustrates the wideband capability of the processor. The high degree of correlation is in no way generated by the process of stacking. In fact, alternate deghosted traces have no common data between them. This degree of correlation is expected if the following conditions are fulfilled by the data:

(1) constant charge size,

(2) elimination of horizontally traveling energy (surface waves, etc.),

(3) receiver position constant for all shots,

(4) medium in which the shots occur is homogeneous,

(5) ghost reflections eliminated.

Conditions (1) and (3) were accomplished in the field, (2) was achieved by the recording array and velocity filtering, (4) implies that the same wavelet was put into the ground for each shot which was substantiated by monitoring the uphole wavelet, and a velocity survey, showing constant velocity between 30 ft ar[redacted]0 ft, and (5) was accomplished by the present process.

To further evaluate the ghost problem and to understand its relationship to the near-surface, the process was applied to the data to enhance ghost energy and reject primaries. This processing is shown as the last seven traces in Figure 6. The amplitude of the deprimaried traces has been boosted by about 6 db to bring them up to the level of the input and deghosted traces. Notice there is only ghost moveout present. Furthermore, the ghost reflections appear to be simply related to the primaries. For example, the strong ghost at about .35 sec is the mirror image of its primary, and has the correct delay for a ghost off the base of the weathering. There is a second ghost following the aforementioned by 30 msec, which would correspond to a ghost off the surface. Thus, it appears that the ghosting mechanism in this area consists of two specular reflectors, one at the base of the weathering layer and the other at the surface. These observations may be confirmed in a quantitative manner through the use of both correlation functions, and the estimation of the impulse response of the near-surface obtained from computing the optimum linear operator for transforming the deghosted traces back into the original ghosted traces.

GHOST ANALYSIS USING CORRELATION FUNCTIONS

The use of the autocorrelation function, and its interpretation for a single ghosting horizon has been discussed by Lindsey (1960). His analysis can be readily extended to more complex ghosting situations. Of particular interest here is the predicted autocorrelation function for a double ghost mechanism.

Let the trace represented by primary energy only be $p(t)$. The ghosted trace resulting from two near-surface reflectors (above the shot) is approximately given by

$$g(t) = p(t) - \alpha_1 p(t - \tau_1) - \beta p(t - \tau_2) \quad (6)$$

τ_1 = two-way traveltime from shot to the first ghost generator.

τ_2 = two-way traveltime from shot to the second ghost generator.

α_1 = reflection coefficient of the first reflector, and

β = apparent reflection coefficient of the second reflector.

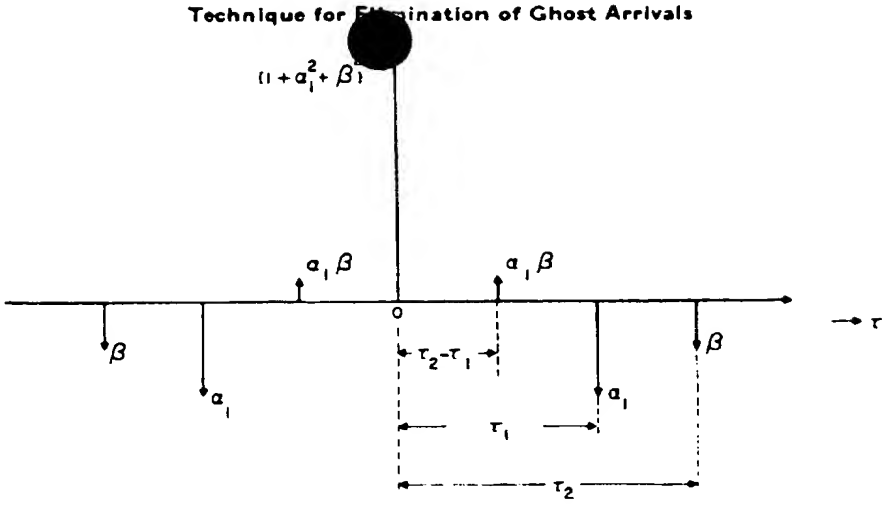

FIG. 7. Impulse autocorrelation function for primary plus double-ghost problem.

The true reflection coefficient of the second reflector, α_2, is related to β by $\alpha_2=\beta/(1-\alpha_1^2)$. In the above, multiple reflections between the two reflectors have been neglected.

The correlation function $\phi(\tau)$ for the ghosted trace is given by

$$\phi_{p+g}(\tau) = \frac{1}{T_2 - T_1}\int_{T_1}^{T_2} g(t)g(t+\tau)dt.$$

Substituting in the above for $g(t)$ given by equation (6), expanding and collecting like terms, the ghosted autocorrelation function may be written as a sum of seven terms:

$$\begin{aligned}\phi_{p+g}(\tau) = {} & (1+\alpha_1^2+\beta^2)\phi_p(\tau) \\ & + \alpha_1\beta\phi_p(\tau-\tau_2+\tau_1) \\ & + \alpha_1\beta\phi_p(\tau+\tau_2-\tau_1) \\ & - \alpha_1\phi_p(\tau-\tau_1) - \alpha_1\phi_p(\tau+\tau_1) \\ & - \beta\phi_p(\tau-\tau_2) - \beta\phi_p(\tau+\tau_2) \quad (7)\end{aligned}$$

where

$$\phi_p(\tau) = \frac{1}{T_2 - T_1}\int_{T_1}^{T_2} p(t)p(t+\tau)dt$$

is the autocorrelation function of the primary reflection sequence. Expression (7) may also be written as the convolution of $\phi_p(\tau)$ with a sequence of impulses as

$$\phi_{p+g}(\tau) = \int_{-\infty}^{\infty} \phi_p(t)h(\tau-t)dt,$$

with

$$\begin{aligned}h(\tau) = {} & (1+\alpha_1^2+\beta^2)\delta(\tau) + \alpha_1\beta\delta(\tau-\tau_2+\tau_1) \\ & + \alpha_1\beta\delta(\tau+\tau_2-\tau_1) - \alpha_1\delta(\tau-\tau_1) \\ & - \alpha_1\delta(\tau+\tau_1) - \beta\delta(\tau-\tau_2) \\ & - \beta\delta(\tau-\tau_2). \quad (8)\end{aligned}$$

It is more instructive to examine $h(\tau)$, the impulse autocorrelation, than $\phi_{p+g}(\tau)$ since the latter contains the smearing effects of the reflection wavelet.

The impulse autocorrelation function $h(\tau)$ for primary and double-ghost situation is shown in Figure 7. Note that if $\beta\to 0$, the autocorrelation function reduces to that given by Lindsey (1960) after convolution with the primary autocorrelation function $\phi_p(\tau)$. The addition of a second ghost reflector results in two additional features in the structure of the correlation function as seen in Figure 7. The negative spike of amplitude β at $\pm\tau_2$ sec results from the correlation of primary and ghost reflections separated in time by τ_2 sec, that is, the second set of ghosts; while the positive feature of amplitude $\alpha_1\beta$ at $\pm(\tau_2-\tau_1)$ seconds is due to the correlation between the two ghosts themselves. The degree to which these features may be seen on an autocorrelation function depends, of course, upon the resolving power of the primary correlation $\phi_p(\tau)$. If the latter is very nearly a delta function itself, then our picture in Figure 7 would remain essentially unchanged. If, however, $\phi_p(\tau)$ is slowly decaying away from zero lag because of reverberations or

narrow-band signal information, the [illegible]ur impulse representation would be severely distorted after convolution, and our ability to identify particular wiggles in the correlation function with ghosting would be practically nil.

The autocorrelation functions were computed for the input traces in Figure 6 and are shown in Figure 8 arranged in order of decreasing hole depth. Only the positive half of the correlation function is shown, it being sym[illegible]ic about zero lag or $\tau=0$. Twice the uphole time, $2T_{uh}$, as determined from the uphole pulse is indicated by an arrow below each correlation function. There is generally good agreement between this time and a trough in the correlation functions predicted for the primary-surface ghost correlation. A second stronger trough can be seen preceding the surface ghost trough by about 30 msec, and

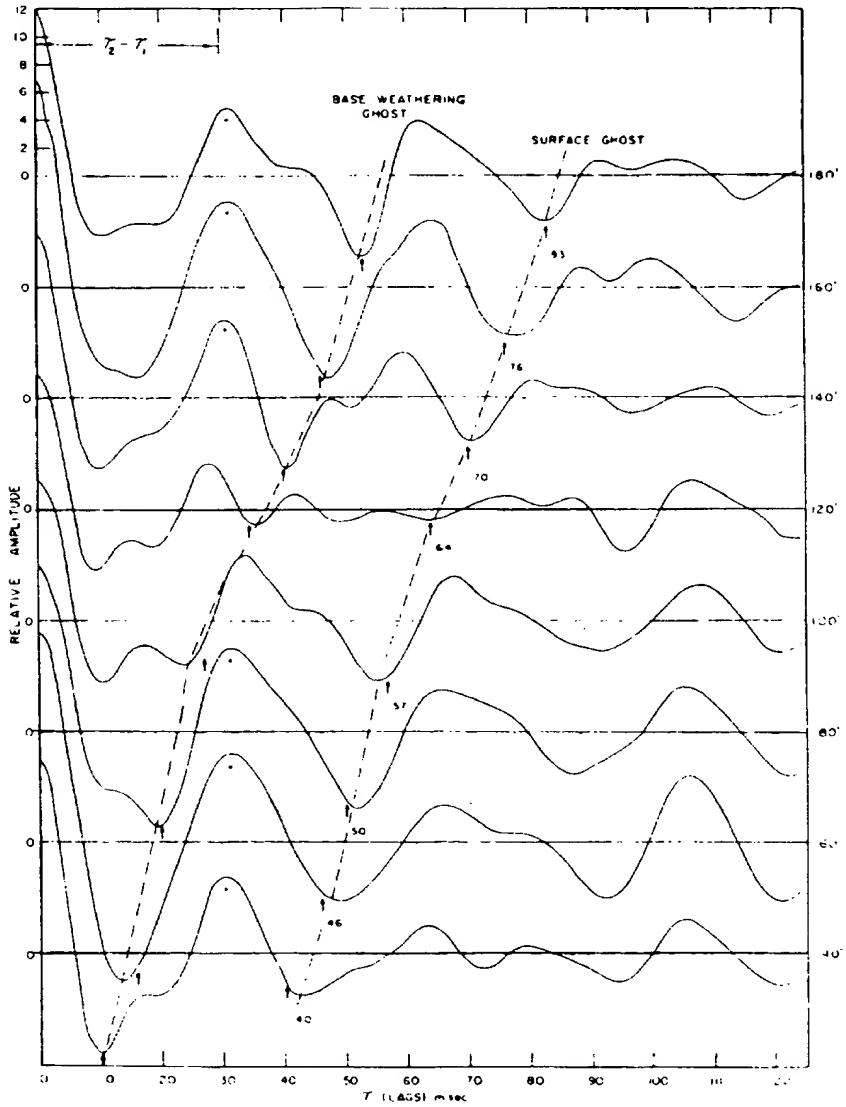

FIG. 8. Autocorrelation functions of uphole traces.

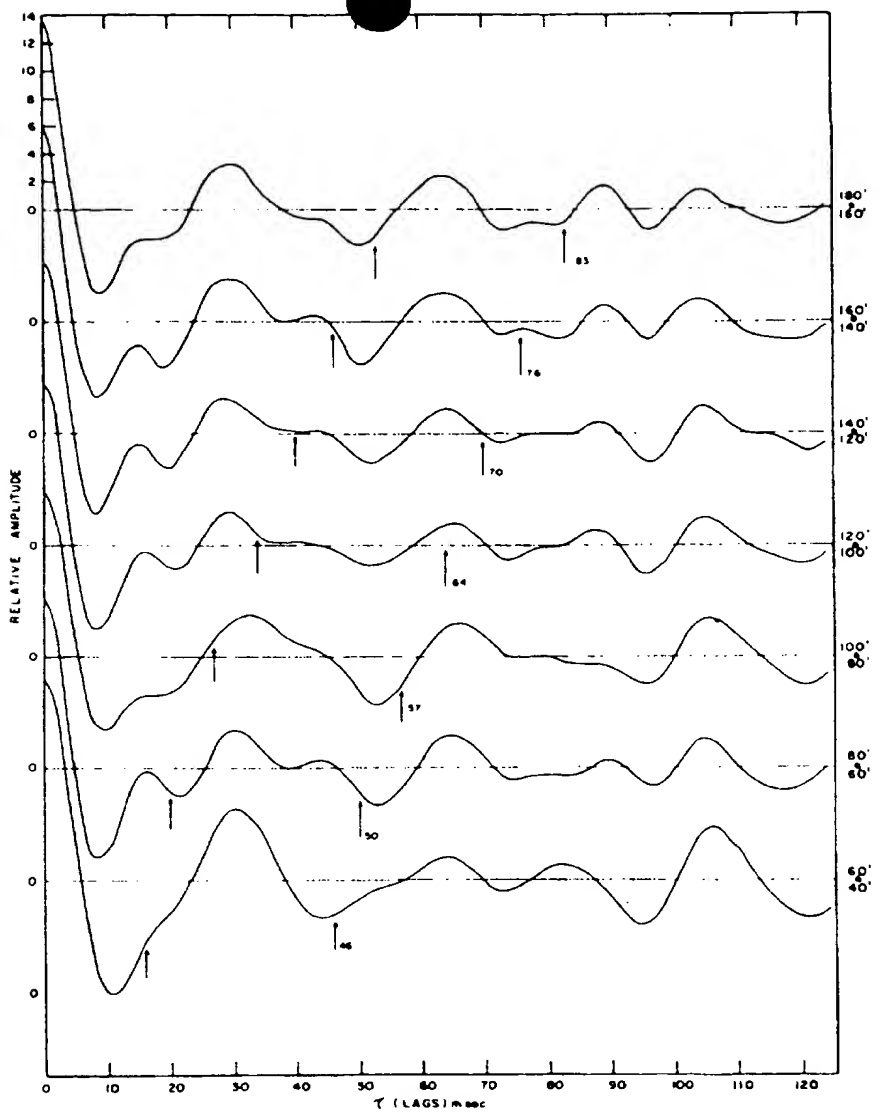

FIG. 9. Autocorrelation functions of deghosted traces.

paralleling the latter's moveout between shot depths. This trough is identified with a base-of-the-weathering ghost reflection, which is the most prominent ghost on the records. There is also a positive correlation at about 30 msec independent of depth, that is, predicted by Figure 7 for two ghosts separated by 30 msec.

The correlation functions of the deghosted traces of Figure 6 are shown in Figure 9. The two troughs associated with ghosting which move across the correlations in Figure 8 are no longer evident. In fact, the residual wiggles show good reproducibility from shot depth to shot depth with the exception of the shallower shots. They represent the structure in the autocorrelation of the effective seismic wavelet, $\phi_p(\tau)$, which is independent of shot depth for reasonable depths.

Several additional features become clear with

the before and after correlations [redacted]ures 8 and 9. The 120-ft ghosted correlation function shows anomalous lack of correlation for τ greater than 30 msec. At this depth, however, the ghost troughs coincide with peaks in the primary correlation $\phi_p(\tau)$ causing destructive interference. The primary autocorrelation functions in Figure 9 do have an intrinsic peak at about 30-msec lag, however, this peak is reduced from Figure 8 indicating that the positive correlation of the two ghosts contributed to its amplitude.

It becomes evident what difficulties might be encountered in attempting to use amplitude information from the ghosted correlation functions to estimate reflection coefficients and near-surface filtering effects on the ghost reflections. Not having to specify these parameters makes shot-stacking a particularly attractive deghosting technique.

ESTIMATE OF NEAR-SURFACE REFLECTION RESPONSE

Once we have obtained a ghost-free estimate of the subsurface reflection sequence, we can work backwards and achieve a quantitative description of the near-surface reflection complex. This is accomplished by computing the operator or filter which transforms a deghosted trace into one of the ghosted traces from whence it came. The impulse response or time-domain representation of this operator should embody the effects of the near-surface on the reflection seismograms, e.g., the cause of the ghosting.

Mathematically, we seek the operator $h(\tau)$ which will transform a ghost-free trace $p(t)$ back into a ghosted trace $g(t)$ or which satisfies the relation,

$$g(t) = \int_{-\infty}^{\infty} p(\tau)h(t-\tau)d\tau. \qquad (9)$$

At this point the reader may wonder if he is not caught in a vicious circle of first removing ghosts and then replacing them in the data. To expel any such fears a word of explanation is in order. Recall that the present process by design only requires knowledge of the difference in uphole times for its implementation. No other information about the ghosts is required such as: reflection coefficients, primary-ghost time lag, near-surface filtering effects, or details of the ghosting mechanism. Therefore, these parameters which are interesting from the standpoint of studying the near-surface and its effec[redacted]he reflection seismogram do not automatically drop out of the processing. They may be inferred, of course, by visually examining the traces before and after deghosting, and computing correlation functions and the like. The integral equation (9) however, provides a quantitative measure of these near-surface parameters in terms of the unknown function $h(t)$.

The least-squares estimate of $h(t)$ may be obtained from $g(t)$ and the deghosted estimate of the primary reflection sequence $\tilde{p}(t)$. That is, we seek the filter $\hat{h}(t)$ which minimizes the mean-square error,

$$\overline{e(t)^2} = \frac{1}{2T}\int_{-T}^{T}[g(t) - \hat{h}(t) * \tilde{p}(t)]^2 dt \qquad (10)$$

where * denotes convolution. Solutions of equation (10) for discrete data are given by Levinson, 1947, and more recently by Levin, 1960, and Robinson, 1963.

In matrix form, the least-squares estimate of $\hat{h}(t)$ is,

$$\begin{bmatrix} \phi_p(0) & \phi_p(1) & \phi_p(2) & \cdots & \phi_p(N) \\ \phi_p(1) & \phi_p(0) & \phi_p(1) & \cdots & \\ \vdots & & & & \\ \phi_p(N) & & \cdots & & \phi_p(0) \end{bmatrix} \begin{bmatrix} \hat{h}(0) \\ \hat{h}(1) \\ \hat{h}(2) \\ \vdots \\ \hat{h}(N) \end{bmatrix} = \begin{bmatrix} \phi_{pg}(0) \\ \phi_{pg}(1) \\ \phi_{pg}(2) \\ \vdots \\ \phi_{pg}(N) \end{bmatrix} \qquad (11)$$

where $\phi_p(i)$ is the ith lag autocorrelation of $\tilde{p}(t)$, and $\phi_{pg}(i)$ is the ith lag crosscorrelation of $\tilde{p}(t)$, and $g(t)$. The special symmetry properties of the correlation matrix in (11) allow an iterative solution for the filter weights $\hat{h}(i)$. That is, the solution vector $[\hat{h}(i)]^T$ can be obtained by operations on the previous vector $[\hat{h}(i-1)]^T$ without actually inverting the $i \times i$ correlation matrix, as demonstrated by Levinson, 1947.

Figure 10 shows the operator $\hat{h}(t)$ calculated for several different shot depths at SP 2.

At each depth represented, the operator was

computed from a deghosted trace and the ghosted trace corresponding to that depth. The spike in the operators at $t=0$ simply reproduces the primary events when convolved with $p(t)$. The first strong negative trough produces the base-of-weathering ghosts, and the second shallow, broad trough correlating with twice the uphole time gives rise to the surface ghost. As also observed on the autocorrelation functions, this double set of troughs is separated by 30 msec. The base-of-the-weathering trough remains constant up the hole in both amplitude and character, whereas the shallow surface ghost trough exhibits sizeable waveform fluctuations from shot to shot. This may be indicative of the noise level of the data.

The reflection coefficients α_1 and β defined in equation (6) were estimated from the operators in Figure 10 by taking the ratio of ghost trough to primary peak at $t=0$. Admittedly, this may be a crude approximation to the true reflection coefficients in view of the difference in frequency content between the base-of-weathering and surface ghost trough. Clearly β and α_1 are frequency dependent, or at least our simple model of two sharp ghosting horizons forces them to be. Since we have not allowed for frequency dependent absorption within the weathering layer, any effects due to absorption are necessarily lumped in the parameter β. Keeping these facts in mind, the average reflection coefficients obtained from the near-surface responses in Figure 10 are:

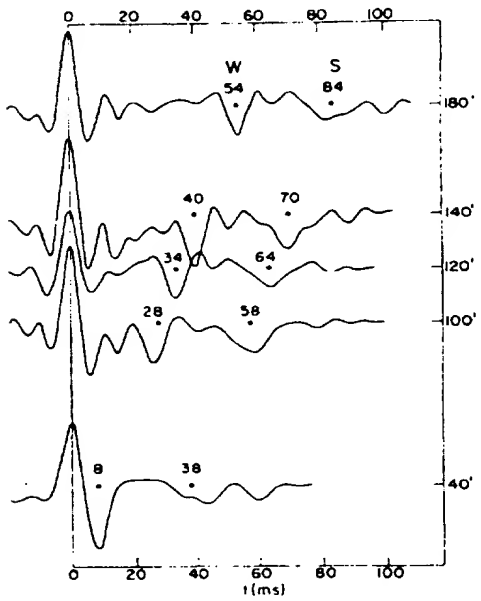

FIG. 10. Near-surface response estimate obtained for several shot depths.

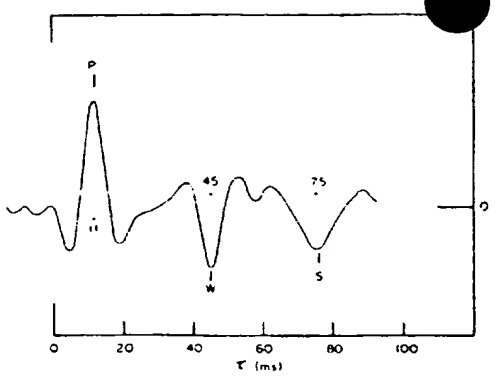

FIG. 11. Near-surface response estimate obtained from transforming the 180-ft deghosted trace into the 120-ft original trace.

$$\overline{\alpha_1} = .47,$$

$$\bar{\beta} = .28,$$

giving for the surface reflection coefficient

$$\overline{\alpha_2} = \frac{\beta}{1 - \alpha_1^2} = \frac{.28}{.78} = .36.$$

These estimates provide a lower limit for the reflection coefficients because of the imperfect rejection of ghost energy and because of noise correlation between deghosted and original traces.

To reduce the effect of residual ghost and noise correlation, the optimum filter to transform the 180-ft deghosted trace into the 120-ft original trace was computed. The filter, limited to about 70 cps on the high side, is shown in Figure 11. The reduction of "primary" correlation relative to ghost correlation is apparent. Crudely compensating for the low-frequency drift in the operator, the values,

$$\overline{\alpha_1} \quad .6$$

$$\bar{\beta} \quad .4$$

$$\overline{\alpha_2} \quad .6$$

are obtained. This yields a model indicated in Figure 12.

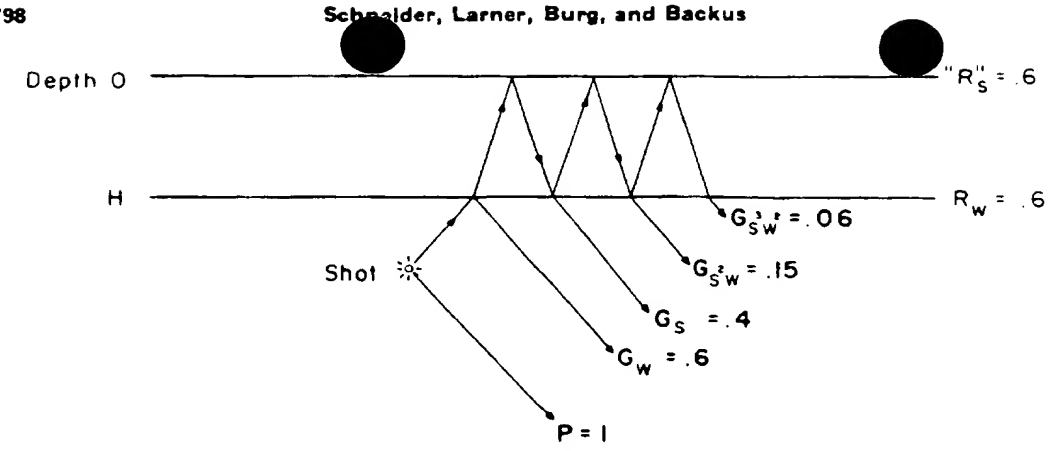

FIG. 12. Two-interface model for near-surface.

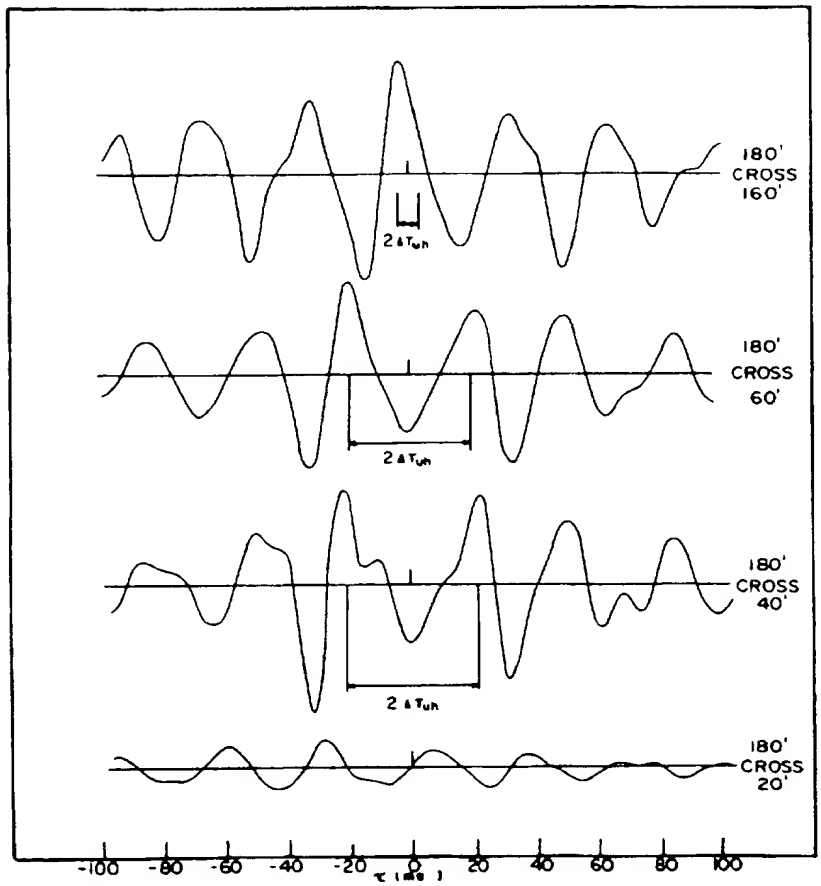

FIG. 13. Crosscorrelation functions computed between different shotpoints for the original velocity-filtered uphole traces.

The fact that the effective reflection coefficient of the surface is less than one (i.e. $R_s \approx .6$) is presumably due to energy dissipation in the weathering layer. This is further supported by the apparent lack of high frequency (above 50 cps) in the weathering ghost.

The simple two-interface discrete model shown in Figure 12 yields a result that the total energy in the ghost complex should be about 54 percent of the total initially down-traveling wave, $(.6^2+.4^2+.15^2+.06^2=.54)$. The adequacy of this simple model can be further tested by examination of the crosscorrelation function computed between different shot depths for the original velocity filtered traces, shown in Figure 13. As exemplified in the crosscorrelation between the 180-ft shot and the 40-ft shot, all of the primary energy should correlate at a lag $\tau = -\Delta T_{uA}$, and all of the initially up-traveling energy should correlate at a lag $\tau = +\Delta T_{uA}$, no matter how complex the ghosting mechanism is. The 180–160 ft correlation is uninterpretable because of the small ΔT_{uA} involved. The 20-ft shot is in the weathering and yields a very unreliable correlation. The two center correlations in Figure 13 suggest that the initially up-going energy contributes about 80 percent as much energy to the reflection record as the initially down-going energy. This compares with a 54 percent figure accounted for by analysis on the basis of the simple two-reflector model in Figure 12. The 80 percent figure suggests that about 20 percent of the initially up-going energy in the reflection-record frequency range is dissipated in the weathering layer or scattered by undulation in the boundaries of the upper reflectors.

The major portion of the analysis was focused on SP 2. However, the SP 1 data yielded similar findings, with the exception that the ghosting appeared somewhat more complex. This was evident on the uphole traces as well as the autocorrelation functions, which were less interpretable from a ghosting standpoint than those in Figure 8 from SP 2. After deghosting, the SP 1 traces correlated very well with the SP 2 deghosted traces.

The estimate of the near-surface reflection response at SP 1 obtained from transforming deghosted into ghosted traces revealed differences in the near-surface response between SP 1 and SP 2. Figure 14 shows a comparison of the near-surface response estimates obtained at the two shotpoints for the 180-ft shot depth. The portions of the operators relating to primaries are almost identical. Twice the uphole times indicated by S are significantly different at the two shotpoints, yet the base-of-the-weathering reflector remains essentially fixed, therefore, the traveltime through the weathering at SP 1 is about 7 msec shorter than at SP 2. The base-of-the-weathering ghost trough at SP 1 is of comparable strength to the SP 2 trough, but does not possess the symmetry of the latter. Furthermore, $2T_{uA} = S$ at SP 1 does not correspond to a well-defined ghost trough; and finally an additional strong positive feature appears at the first reverberation time within the weathering layer. Therefore, it is likely that the total interval from about 50 to 90 msec at SP 1 represents ghosting, the details of which are not resolved as simple troughs or peaks but rather form a complex interference.

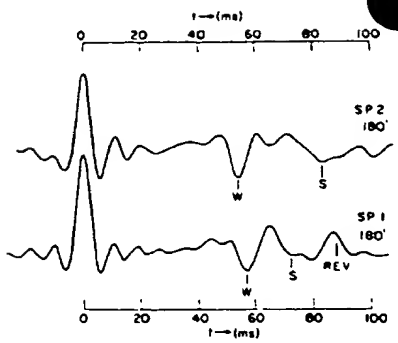

FIG. 14. Comparison of near-surface response estimates obtained at SP 1 and SP 2 for the 180-ft shot.

CONCLUSIONS

A new deghosting technique is presented which utilizes two shots at different depths. It differs from conventional stacking in that separate filters are applied to the two shots before stacking. The filters are designed in an optimum manner to enhance initially down-traveling energy and reject initially up-traveling energy. The resulting process has wide-band ghost reject and signal-preservation characteristics. No specific knowledge of the ghost mechanism is required for its implementation other than, (1) determining the difference in uphole times, (2) assuming a spectral content for signal and noise, usually "white" over

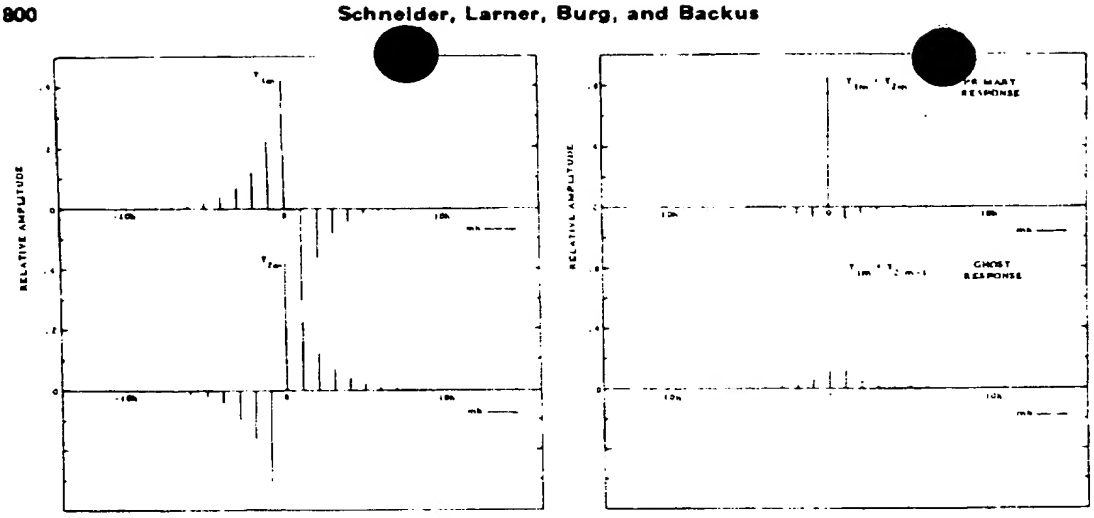

FIG. 15. Left half of the figure shows the sampled impulse response of the deghosting filters, and the right half shows the impulse response for primaries and ghosts obtained by suitably adding the filter responses.

the frequency range of interest, and (3) insuring that both shots are below the ghosting mechanism. The method will handle ghosting from a reflection complex or ghosts from a single reflector equally well.

The degree of primary and ghost energy separation achievable with the present process permits the quantitative investigation of the near-surface reflection response by computing the operator which transforms the deghosted into the ghosted trace.

ACKNOWLEDGMENTS

We wish to acknowledge the assistance of Earl C. Wisler in early experimental applications of this technique. We also thank Texas Instruments Incorporated and Geophysical Service Inc. for permission to publish this paper.

REFERENCES

Burg, J. P., Three-dimensional filtering with an array of seismometers: Geophysics, v. 29, p. 693–713.

Embree, P., Burg, J. P., and Backus, M. M., 1963, Wide-band velocity filtering—the Pie-Slice process: Geophysics, v. 28, p. 948–974.

Foster, M. R., and Sengbush, R. L., (to be published) Design of sub-optimum filter systems for multi-trace seismic data processing: Geophysical Prospecting.

Hammond, J. W., 1962, Ghost elimination from reflection records: Geophysics, v. 27, p. 48–60.

Levin, M. J., 1960, Optimum estimations of impulse response in the presence of noise: IRE Transactions C.T., v. CT-7, p. 50–56.

Levinson, N., 1947, A heuristic exposition of Wiener's mathematical theory of prediction and filtering: Journal of Math. and Physics, v. 26, p. 110–119.

Lindsey, J. P., 1960, Elimination of seismic ghost reflections by means of a linear filter: Geophysics, v. 25, p. 130–140.

Musgrave, A. W., Ehlert, G. W., and Nash, D. M., Jr., 1958, Directivity effect of elongated changes: Geophysics, v. 23, p. 81–96.

Robinson, E. A., 1963, Mathematical development of discrete filters for the detection of nuclear blasts: Jour. Geoph. Res., v. 63, p. 5559–5567.

Sparks, N. R., and Silverman, D., 1953, Pressure field around distributed charges: Seventh Annual Midwestern Meeting of the Society of Exploration Geophysicists, Dallas, Texas, November 12–13.

Spieker, L. J., Burg, J. P., Backus, M. M., and Strickland, L., 1961, Seismometer array and data processing system: Final Report Phase I, AFTAC contract AF 33(600)-41840, Project VT/077.

Wiener, N., 1949, Extrapolation interpolation and smoothing of stationary time series: New York, John Wiley and Sons, p. 104–116.

APPENDIX A

LEAST-SQUARES TWO-CHANNEL FILTER DESIGN

The classical least-squares technique is applied to two-channel sampled time functions for optimum-filter design by an obvious extension of Levinson's (1947) single-channel treatment.

Consider the two-channel time functions $f_1(t)$ and $f_2(t)$ to be represented by their sampled values at points $t = kh$, where h is the sample period and k is an index. Let the sampled functions $f_1(kh)$ and $f_2(kh)$ be regarded as the sequences b_{1k} and b_{2k} representing signal and noise, that is:

$$b_{1k} = S_{1k} + N_{1k},$$

$$b_{2k} = S_{2k} + N_{2k},$$

where

S_{1k} = signal on channel 1,

S_{2k} = signal on channel 2,

N_{1k} = noise on channel 1,

N_{2k} = noise on channel 2.

We wish to determine the pair of linear filters which, when convolved, respectively, with the input sequences b_{1k} and b_{2k} and summed, will give an output as similar as possible to the desired signal on one of the input channels, say S_{1k}. The filter sequences Y_{1k} and Y_{2k} are designed such that the total power in the error signal

$$E_k \equiv S_{1k+p} - \sum_{n=0}^{M} Y_{1n} b_{1k-n} - \sum_{n=0}^{M} Y_{2n} b_{2k-n} \qquad \text{(A-1)}$$

is minimized. The power in the error signal is given by the sum of the squares of the E_k's, or stated in formula

$$I = \lim_{N\to\infty} \frac{1}{2N+1} \sum_{k=-N}^{N} E_k^2$$

$$= \lim_{N\to\infty} \frac{1}{2N+1} \sum_{k=-N}^{N} (S_{1k+p})^2 - 2 \sum_{n=0}^{M} Y_{1n} \lim_{N\to\infty} \frac{1}{2N+1} \sum_{k=-N}^{N} S_{1k+p} b_{1k-n}$$

$$- 2 \sum_{n=0}^{M} Y_{2n} \lim_{N\to\infty} \frac{1}{2N+1} \sum_{k=-N}^{N} S_{1k+p} b_{2k-n}$$

$$+ 2 \sum_{n=0}^{M} \sum_{m=0}^{M} Y_{1n} Y_{2m} \lim_{N\to\infty} \frac{1}{2N+1} \sum_{k=-N}^{N} b_{1k-n} b_{2k-m}$$

$$+ \sum_{n=0}^{M} \sum_{m=0}^{M} Y_{1n} Y_{1m} \lim_{N\to\infty} \frac{1}{2N+1} \sum_{k=-N}^{N} b_{1k-n} b_{1k-m}$$

$$+ \sum_{n=0}^{M} \sum_{m=0}^{M} Y_{2n} Y_{2m} \lim_{N\to\infty} \frac{1}{2N+1} \sum_{k=-N}^{N} b_{2k-n} b_{2k-m}, \qquad \text{(A-2)}$$

which is to be minimized with respect to the Y_{1k}'s and Y_{2k}'s.

Equation (A-2) may be simplified by introducing the correlation functions.

The autocorrelation function for a sampled time function is defined as,

$$R_a(k) = \lim_{N\to\infty} \frac{1}{2N+1} \sum_{s=-N}^{N} a_s a_{s-k},$$

and the crosscorrelation function between two sampled time functions as

$$R_{ba}(k) = \lim_{N\to\infty} \frac{1}{2N+1} \sum_{s=-N}^{N} (a_s b_{s-k}) = R_{ab}(-k).$$

Substituting the correlation functions into equation (A-2) we have:

$$I = R_{s_1}(0) - 2 \sum_{n=0}^{M} Y_{1n} R_{b_1 s_1}(n+p) - 2 \sum_{n=0}^{M} Y_{2n} R_{b_2 s_1}(n+p) + 2 \sum_{n=0}^{M} \sum_{m=0}^{M} Y_{1n} Y_{2m} R_{b_2 b_1}(m-n) + \sum_{n=0}^{M} \sum_{m=0}^{M} Y_{1n} Y_{1m} R_{b_1}(m-n) + \sum_{n=0}^{M} \sum_{m=0}^{M} Y_{2n} Y_{2m} R_{b_2}(m-n). \qquad \text{(A-3)}$$

For I to be a minimum with respect to the Y_{1k}'s and Y_{2k}'s we must have

$$\frac{\partial I}{\partial Y_{1k}} = 0 \qquad k = 0, 1, 2 \cdots M$$

$$\frac{\partial I}{\partial Y_{2k}} = 0$$

or

$$\frac{\partial I}{\partial Y_{1k}} = -2R_{b_1a_1}(k+p) + 2\sum_{m=0}^{M} Y_{2m}R_{b_2b_1}(m-k) + 2\sum_{m=0}^{M} Y_{1m}R_{b_1}(k-m) = 0$$

$$\frac{\partial I}{\partial Y_{2k}} = -2R_{b_2a_1}(k+p) + 2\sum_{m=0}^{M} Y_{1m}R_{b_2b_1}(k-m) + 2\sum_{m=0}^{M} Y_{2m}R_{b_2}(k-m) = 0 \quad \text{(A-4)}$$

This system of equations may be written in matrix form as

$$\begin{bmatrix} r_0 & r_1 & r_2 & \cdots & r_M \\ r_{-1} & r_0 & r_1 & & \\ r_{-2} & & \cdot & & \\ & & & \cdot & \\ r_{-M} & & & & r_0 \end{bmatrix} \begin{Bmatrix} Y_0 \\ Y_1 \\ \cdot \\ \cdot \\ Y_M \end{Bmatrix} = \begin{Bmatrix} r_p \\ \gamma_{1+p} \\ \gamma_{2+p} \\ \\ \gamma_{M+p} \end{Bmatrix} \quad \text{(A-5)}$$

where each of the r_i's, Y_i's, and γ_j's are submatrices defined as follows

$$r_{m-k} = \begin{bmatrix} R_{b_1}(m-k) & R_{b_2b_1}(m-k) \\ R_{b_1b_2}(m-k) & R_{b_2}(m-k) \end{bmatrix}$$

$$Y_m = \begin{bmatrix} Y_{1m} \\ Y_{2m} \end{bmatrix}$$

$$\gamma_{k+p} = \begin{bmatrix} R_{b_1a_1}(k+p) \\ R_{b_2a_1}(k+p) \end{bmatrix}.$$

Notice also that $r_{m-k} = r^T_{k-m}$.

An iterative solution to (A-5) is also possible (Robinson, 1963) as in the single-channel case. The parameter p in R_i and equation (A-1) relates to whether or not one desires to do filtering, filtering and prediction, or interpolation. If $p=0$, we attempt to extract S_k from knowledge of the b's up to time $t=hk$. If $p>0$, we attempt to predict S_{k+p} ahead in time by $t=hp$ sec, and if $p<0$, we use values of the b's in future time to interpolate the value of S_{k-p}.

Up until now the derivation has been completely general without regard to the deghosting problem. In order to design the deghosting filters on a theoretical model the various correlation functions in (A-4) must be specified.

The signal and noise description for the ghost-reflection problem on a two-channel basis may be adequately specified as:

Shallow shot

$$f_1(t) = P_1(t) + G_1(t) + N_1(t)$$

Deep shot

$$f_2(t) = P_2(t) + G_2(t) + N_2(t)$$

where

$P_{1,2}(t)$ = primary reflection sequence on channel 1, 2,

$G_{1,2}(t)$ = ghost reflection sequence on channel 1, 2,

$N_{1,2}(t)$ = random noise on channel 1, 2.

If the traces $f_1(t)$ and $f_2(t)$ are static-shifted by the difference in uphole time $=\Delta T_{uh}$ then $P_1(t)=P_2(t)=P(t)$, and $G_1(t)=G(t)$, $G_2(t)=G(t-2\Delta T_{uh})$, based on the assumption that both shots are in the same medium below the ghosting horizon. We further assume that the random noise is white with power density level N_0, and is uncorrelated with primaries or ghosts. The final assumption concerns the crosscorrelation of primaries and ghosts. Of course, physically they are correlated as Figure 8 shows, however, the measurement of this correlation is difficult even with good data. Furthermore, the primary ghost correlation can be expected to change drastically in short horizontal distances due to variable near-surface conditions as well as variations in shot depth. From the practical consideration of filter design we neglect the primary ghost correlation and accept the slight loss in filter effectiveness.

With these assumptions, the various auto- and crosscorrelations become in the continuous case:

$$\begin{aligned} R_{b_1}(\tau) &= \phi_p(\tau) + \phi_v(\tau) + N_0\delta(\tau), \\ R_{b_2}(\tau) &= \phi_p(\tau) + \phi_v(\tau) + N_0\delta(\tau), \\ R_{b_1b_2}(\tau) &= \phi_p(\tau) + \phi_v(\tau - 2\Delta T_{uh}), \\ R_{b_2b_1}(\tau) &= \phi_p(\tau) + \phi_v(\tau + 2\Delta T_{uh}), \\ R_{b_1a_1}(\tau) &= \phi_p(\tau), \\ R_{b_2a_1}(\tau) &= \phi_p(\tau). \end{aligned} \quad \text{(A-6)}$$

In order that the filters have a wide-band capability for separating primaries and ghosts we assume that the spectral content of the primaries and ghosts is white over the frequency range of interest. That is, we are not introducing any frequency difference between signal and noise, but rather exploiting only the spatial correlation differences. Thus, the correlations become

$$\phi_p(\tau) = P\delta(\tau),$$
$$\phi_g(\tau) = G\delta(\tau), \qquad \text{(A-7)}$$

where P and G are the signal and ghost-power levels and $\delta(\tau)$ is the delta function.

Figure 15 shows the impulse response of the filters Y_{1m} and Y_{2m} designed by means of equation (A-5), using correlations defined by (A-6) and (A-7) for the following parameters:

$P = 1.0$ primary power level,

$G = 1.0$ ghost power level,

$N_o = .1$ random noise power level,

$2\Delta T_{sh} = 1.0$ times the sample period $= h$,

$M = 20$ number of filter points minus one,

$p = -10$.

The figure also shows the impulse response for primaries obtained by adding $Y_{1m}+Y_{2m}$, and the impulse response for ghosts obtained by shifting and adding $Y_{1m}+Y_{2m-1}$. Note that the response for primaries is very nearly a delta function with maximum side-lobe levels of less than 10 percent of the main peak, whereas the impulse response for ghosts is uniformly small.

The time-domain formulation of the least-square filter problem presented here is clearly superior to a frequency-domain formulation if the resulting filters are to be used as finite digital convolution operators. The reason being that the former provides an optimum finite length operator, whereas the latter yields an optimum amplitude and phase spectrum which must be Fourier transformed and in general truncated in the time domain. In the limit of infinite-length operators, the time and frequency domain results are identical. Inasmuch as filter or operator length is an important economic factor in the implementation of this and other related techniques it is desirable to achieve the maximum effectiveness of the filter with the least number of points. The time-domain solution insures that each of the N-filter points used is optimum. In addition, by examining the mean-square error as a function of number of filter points, it is possible in most problems to select a minimum filter length beyond which the mean-square error essentially levels off. That is, the addition of more points to the filter does not significantly improve its performance in the mean-square-error sense.

The frequency domain on the other hand, if not best suited for digital filter design, does provide physical insight and interpretation that is lacking in equations (A-5) and (A-6).

The frequency-domain solution to multiple time series least-mean-square-error filter problems is contained in Wiener's (1949) original work. Certain important simplifications in the mathematics result when both the past and future of the time series are available for filter design, as is the case of magnetic-tape-recorded seismic data. The solution for the optimum filters $Y_j(f)$ operating on both past and future is (Spieker, Burg, Backus, and Strickland, 1961; Foster and Sengbush, 1964; and Burg, 1964) given by the matrix equation,

$$[S_{ij}(f) + N_{ij}(f)][Y_j(f)] = [S_{ik}(f)]$$
$$i = 1, 2, \cdots, N,$$
$$j = 1, 2, \cdots, N, \qquad \text{(A-8)}$$

where $S_{ij}(f)$ and $N_{ij}(f)$ are the cross-spectral densities between channels i and j for signal and noise, respectively. The column vector $[S_{ik}(f)]$ consists of cross spectral densities between signal in channel i and the desired signal to be estimated at channel k.

The $Y_j(f)$ are, of course, the unknown filters to be applied to each channel in the multichannel signal-extraction process. Equation (A-8) implies that signal and noise are uncorrelated. An additional term in the equation would allow for the latter if it exists.

Using the signal and noise model for the ghosting problem defined by equation (A-6), and transforming to the frequency domain, we have a 2×2 matrix inversion problem for the filters $Y_1(f)$ and $Y_2(f)$;

$$\begin{bmatrix} \Phi_p(f) + \Phi_g(f) + N_0 & \Phi_p(f) + \Phi_g(f)e^{-i2\pi f 2\Delta T_{uh}} \\ \Phi_p(f) + \Phi_g(f)e^{i2\pi f 2\Delta T_{uh}} & \Phi_p(f) + \Phi_g(f) + N_0 \end{bmatrix} \begin{bmatrix} Y_1(f) \\ Y_2(f) \end{bmatrix} = \begin{bmatrix} \Phi_p(f) \\ \Phi_p(f) \end{bmatrix} \quad \text{(A-9)}$$

where

$$\Phi_p(f) = \int_{-\infty}^{\infty} \phi_p(\tau) e^{-i2\pi f \tau} d\tau$$

$$\Phi_g(f) = \int_{-\infty}^{\infty} \phi_g(\tau) e^{-i2\pi f \tau} d\tau.$$

The solutions of (A-9) are,

$$Y_1(f) = \frac{\gamma_R + \gamma_c(1 - e^{-i2\pi f 2\Delta T_{uh}})}{\gamma_R(\gamma_R + 2\gamma_c + 2) + 2\gamma_c(1 - \cos 2\pi f 2\Delta T_{uh})}$$

$$Y_2(f) = Y_1^*(f) \qquad * = \text{complex conjugate.} \quad \text{(A-10)}$$

The γ's are the noise-to-signal-power ratios, that is,

$$\gamma_R = \frac{N_o}{\Phi_p}$$

= random-noise-to-signal-power ratio

$$\gamma_c = \frac{\Phi_g}{\Phi_p}$$

= coherent-noise-to-signal-power ratio.

As previously mentioned, the response for primaries is obtained by adding $Y_1(f)$ and $Y_2(f)$ which yields,

$$Y_1(f) + Y_2(f) = \frac{2\gamma_R + 2\gamma_c(1 - \cos 2\pi f 2\Delta T_{uh})}{\gamma_R(\gamma_R + 2\gamma_c + 2) + 2\gamma_c(1 - \cos 2\pi f 2\Delta T_{uh})}. \quad \text{(A-11)}$$

For $\gamma_R \ll \gamma_c$ the response for primary energy is very nearly equal to unity for all frequencies except at and near the set $f_n = n/2\Delta T_{uh}$, $n = 0, 1, 2 \cdots$ where the response becomes,

$$Y_1(f_n) + Y_2(f_n) = \frac{2}{(\gamma_R + 2\gamma_c + 2)}. \quad \text{(A-12)}$$

The f_n are alias frequencies at which the stack (either conventional or the present process) cannot distinguish between primary and ghost energy. The associated wavelengths $\lambda_n = 2d/n$ are submultiples of twice the vertical shot separation. The denominator of (A-11) which is common to both $Y_1(f)$ and $Y_2(f)$ is essentially a compensation filter to undo the distortion introduced in the primaries as a consequence of ghost attenuation.

The response for ghosts may be obtained in a similar fashion by adding $Y_1(f)$ and $Y_2(f)e^{-i2\pi f 2\Delta T_{uh}}$ giving,

[See A-13 at top of next page]

The latter is small at all frequencies except the set f_n, at which the primary and ghost responses are equal as evidenced by (A-13). At $f_m = m/4\Delta T_{uh}$, $m = 1, 3, 5, 7, \cdots$ equation (A-13) has a zero irrespective of the value of γ_R and γ_c. At these frequencies the ghost energy is 180° out of phase between the two shots and cancellation is effected by simply adding the two traces. This frequency corresponds to the node in the response curves presented in Figure 1. The latter were obtained from equations (A-11) and (A-13) with $\gamma_R = .1$ and $\gamma_c = 1.0$.

It would seem that by allowing the random-noise-to-signal-power ratio γ_R to become arbitrarily small one could effect perfect undistorted separation of primaries and ghosts. That is, equations (A-11) and (A-13) tend to unity and zero, respectively, as $\gamma_R \to 0$. The difficulty, of course, is that the amplitude density of the filters (A-10) becomes infinite at $f = f_n$ for $\gamma_R = 0$. This implies that the impulse response of the filters is not square integrable over the time interval $(-\infty, \infty)$. Indeed, the impulse response of the filters for $\gamma_R = 0$ can be obtained by expanding the periodic frequency spectra (A-10) in a Fourier series and equating the coefficients a_m to delta function amplitudes at $t = m2\Delta T_{uh}$. That is,

$$V_1(f) + V_2(f)e^{-i2\pi f/2\Delta T_{uh}} = e^{-i2\pi f/\Delta T_{uh}} \frac{2\gamma_R \cos 2\pi f \Delta T_{uh}}{\gamma_R(\gamma_R + 2\gamma_c + 2) + 2\gamma_c(1 - \cos 2\pi f 2\Delta T_{uh})}. \quad \text{(A-13)}$$

$$h_1(t) = \sum_{m=-\infty}^{\infty} a_{1m}\delta(t - m2\Delta T_{uh})$$

$$h_2(t) = \sum_{m=-\infty}^{\infty} a_{2m}\delta(t - m2\Delta T_{uh}) \quad \text{(A-14)}$$

where

$$a_{1m} = \begin{cases} +\frac{1}{2} \text{ for } m \leq 0 \\ -\frac{1}{2} \text{ for } m > 0 \end{cases}$$

$$a_{2m} = \begin{cases} -\frac{1}{2} \text{ for } m < 0 \\ +\frac{1}{2} \text{ for } m \geq 0 \end{cases}$$

clearly,

$h_1(t) + h_2(t)$
= response for primaries = $\delta(t)$,

$h_1(t) + h_2(t - 2\Delta T_{uh})$
= response for ghosts = 0.

These filters do not decay with increasing or decreasing time, and are obviously not practical for digital application. The role of random noise in (A-10) clearly provides stability and convergence for the impulse responses such that they may be truncated after a finite number of samples without degradation of the filters. The time-domain formulation circumvents the problem of having to truncate the filters at all by solving (A-5) for optimum N-point filters. The latter will, of course, depend upon γ_R as well as the other parameters used, however, they are the best N-point operators in the mean-square-error sense.